Accurate torque-sensorless control approach for interior permanent-magnet synchronous machine based on cascaded sliding mode observer

Kai-Hui Zhao[1], Chang-Fan Zhang[1], Jing He[1], Xiang-Fei Li[1], Jiang-Hua Feng[2], Jian-Hua Liu[3], Tao Li[3]

[1]*School of Electrical and Information Engineering, Hunan University of Technology, Zhuzhou 412007, People's Republic of China*
[2]*CRRC Zhuzhou Institute Co., Ltd, Zhuzhou 412007, People's Republic of China*
[3]*School of Traffic Engineering, Hunan University of Technology, Zhuzhou 412007, People's Republic of China*
E-mail: zhangchangfan@263.net

Published in *The Journal of Engineering*; Received on 2nd May 2017; Accepted on 16th June 2017

Abstract: To improve the accuracy of torque control for vector control of interior permanent-magnet synchronous machine (IPMSM), this study proposes a torque-sensorless control method based on cascaded sliding mode observer (SMO). First, the active flux model is discussed, which converts the model of IPMSM into the equivalent model of surface-mounted permanent-magnet synchronous machine. Second, to reduce chattering caused by system parameters variations and external disturbances, the cascaded observer is designed, which is composed of a variable gain adaptive SMO and an active flux SMO. The variable gain adaptive SMO is designed to estimate the speed, rotor position and stator resistance in the *d*–*q* reference frame. The active flux SMO is designed to estimate the active flux and torque in the *α*–*β* reference frame. Global asymptotic stability of the observers is guaranteed by the Lyapunov stability analysis. Finally, simulations and experiments are carried out to verify the effectiveness of the proposed control scheme.

1 Introduction

Permanent-magnet synchronous machine (PMSM) has been widely used in industrial applications due to its good dynamic response, high power density, high torque-to-current ratio, and excellent tracking precision [1]. The accurate torque control is the basic requirement for torque control in the application of high-speed train and electric vehicle. However, it is difficult to attain this target because of the variations of interior PMSM (IPMSM) parameters.

To achieve the high-precision torque control for vector control of PMSM, many methods are proposed to estimate load torque, such as the direct calculation method, the full-order and reduced-order observer, the model reference adaptive system, Kalman filters, parameters estimating strategy and so on. A parameter estimation method has been proposed to achieve accurate torque control for the IPMSM by maximum torque per ampere (MTPA) control scheme in [2]. A load torque observer of Kalman filter has been proposed to form forward compensation for surface-mounted PMSM (SPMSM) in [3, 4]. A model reference adaptive identification method of torque closed-loop control has also been proposed in [5]. A load torque observer and a load torque derivatives observer are designed based on the sliding-mode control method in [6]. The accurate torque control method of IPMSM is proposed by parameters estimation in [7].

To achieve high-precision torque control for vector control of PMSM, it is necessary to obtain the speed or position by mechanical sensors. However, it performances tend to be poor. To overcome the drawbacks of the mechanical sensor, and achieve sensorless operation, several algorithms have been suggested in the recent literature [8–16]. Sensorless control can achieve the rotor position and speed exploiting the voltage and current. The benefits of sensorless control are reduced the maintenance, the complexity and the size of PMSM, and increased the reliability. There are two kinds of sensorless controls: the signal injection [8–10] and the fundamental models of PMSM [10–16].

Considering the advantages of sliding-mode control and 'active flux' concept, a torque-sensorless control method is proposed for vector control of IPMSM in this paper. Sliding-mode control [17–23] is an attractive algorithm due to several features, such as robustness of system parameter uncertainties and external disturbance, the ability to handle inaccurate mathematical model. To reduce chattering phenomenon caused by parameter variations and external disturbances of PMSM, the cascaded observer is designed, which is composed of a variable gain adaptive sliding mode observer (SMO) and an active flux SMO. The variable gain adaptive SMO is designed to estimate the speed and stator resistance in the *d*–*q* reference frame. The estimated speed and stator resistance are then imputed to the active flux SMO. The 'active flux' concept [24–29] provides alternatives to convert the model of IPMSM into an equivalent model of SPMSM. The active flux SMO is designed with sigmoid function to estimate the active flux and calculate the torque in the *α*–*β* reference frame. Combining the torque command, the torque-sensorless control system of PMSM is constituted. Simulation and experimental results demonstrate the feasibility of the proposed control method.

The remaining of this paper is organised as follows: The system description is described in Section 2, and the unified PMSM model is derived in the same section. A variable gain adaptive SMO is designed in Section 3, and the SMO of active flux is designed in Section 4. The simulation and experimental results are shown in Section 5. A brief conclusion is given in Section 6.

2 System description

This section briefly demonstrates the mathematical model of SPMSM and IPMSM. IPMSM model can be converted into an equivalent SPMSM model by 'active flux'. Then, the unified PMSM model can be derived.

2.1 Mathematical model of SPMSM in the α–β reference frame

The stator voltage equations of the PMSM in the *α*–*β* reference frame are as follows [30]:

$$\begin{cases} u_\alpha = R_s i_\alpha + \dfrac{\mathrm{d}\psi_\alpha}{\mathrm{d}t} \\ u_\beta = R_s i_\beta + \dfrac{\mathrm{d}\psi_\beta}{\mathrm{d}t} \end{cases} \tag{1}$$

doi: 10.1049/joe.2017.0160

where ψ_α and ψ_β are the α–β axis stator flux linkages, respectively, and given by the following equations in SPMSM:

$$\begin{cases} \psi_\alpha = L_s i_\alpha + \psi_{r\alpha} \\ \psi_\beta = L_s i_\beta + \psi_{r\beta} \end{cases} \tag{2}$$

where $\psi_{r\alpha}$ and $\psi_{r\beta}$ are the α–β axis rotor flux linkages, respectively, and $\psi_{r\alpha} = \psi_r \cos\theta_e$, $\psi_{r\beta} = \psi_r \sin\theta_e$.

Substituting (2) into (1), the equations of SPMSM in the α–β axis reference frame can be expressed as follows:

$$\begin{cases} \dfrac{di_\alpha}{dt} = -\dfrac{R_s}{L_s} i_\alpha + \dfrac{1}{L_s} u_\alpha + \dfrac{\omega_e}{L_s} \psi_{r\beta} \\ \dfrac{di_\beta}{dt} = -\dfrac{R_s}{L_s} i_\beta + \dfrac{1}{L_s} u_\beta - \dfrac{\omega_e}{L_s} \psi_{r\alpha} \end{cases} \tag{3}$$

In (1)–(3), u_α, u_β, i_α and i_β are the α–β axis stator voltages (V) and currents (A), respectively. L_s is the inductance, R_s is the stator resistance (Ω) and ψ_r is the amplitude of the permanent-magnet flux linkage (Wb), ω_e is the electrical angular velocity (rad/s), θ_e is the electrical angular (rad).

2.2 *Mathematical model of IPMSM in the* d–q *reference frame*

The stator voltage equations of PMSM in the d–q reference frame are as follows [30]:

$$\begin{cases} u_d = R_s i_d + \dfrac{d\psi_d}{dt} - \omega_e \psi_q \\ u_q = R_s i_q + \dfrac{d\psi_q}{dt} + \omega_e \psi_d \end{cases} \tag{4}$$

where ψ_d and ψ_q are the d–q axis stator flux linkages, respectively, and given by the following equations in SPMSM:

$$\begin{cases} \psi_d = L_d i_d + \psi_r \\ \psi_q = L_q i_q \end{cases} \tag{5}$$

Substituting (5) into (4), considering ψ_r can be regarded as time invariant in a short-time period, so we get $d\psi_r/dt \simeq 0$. The equations for IPMSM in the d–q axis reference frame can be expressed as follows:

$$\begin{cases} \dfrac{di_d}{dt} = -\dfrac{R_s}{L_d} i_d + \omega_e \dfrac{L_q}{L_d} i_q + \dfrac{u_d}{L_d} \\ \dfrac{di_q}{dt} = -\dfrac{R_s}{L_q} i_q - \omega_e \dfrac{L_d}{L_q} i_d + \dfrac{u_q}{L_q} - \omega_e \dfrac{\psi_r}{L_q} \end{cases} \tag{6}$$

The torque equation of PMSM can be expressed as

$$T_e = \frac{3}{2} n_p \left[\psi_r i_q + \left(L_d - L_q \right) i_d i_q \right] \tag{7}$$

In (4)–(7), u_d, u_q, i_d, i_q, L_d and L_q represent the d–q axis stator voltages (V), currents (A) and inductances (Wb), respectively, ($L_d < L_q$), R_s is the stator resistance (Ω), ψ_r is the amplitude of the magnet flux linkage (Wb), ω_e is the electrical angular velocity (rad/s), θ_e is the electrical angular (rad) and n_p is the number of pole pairs.

2.3 *Active flux model*

Active flux has been defined in the literature [24–29] as

$$\psi_{ext} = \psi_r + (L_d - L_q) i_d \tag{8}$$

where ψ_{ext} represents the active flux, which is a sum of two terms – the conventional permanent-magnet flux linkage and a flux linkage due to saliency [25]. This active flux is the fictitious permanent-magnet flux linkage of an IPMSM.

Equation (7) can now be expressed as

$$T_e = \frac{3}{2} n_p \psi_{ext} i_q \tag{9}$$

Substituting (8) into (5), (5) can be written as

$$\begin{cases} \psi_d = L_q i_d + (L_d - L_q) i_d + \psi_r = L_q i_d + \psi_{ext} \\ \psi_q = L_q i_q \end{cases} \tag{10}$$

Active flux components in the d–q axis reference frame are as follows:

$$\begin{cases} \psi_{ext,d} = \psi_d - L_q i_d = \psi_r + \left(L_d - L_q \right) i_d = \psi_{ext} \\ \psi_{ext,q} = \psi_q - L_q i_q = 0 \end{cases} \tag{11}$$

Analysis of (11) indicates that the active flux is aligned along the d-axis as is the permanent-flux linkage. Hence, the active flux components in the α–β axis reference frame are as follows. This is shown in Fig. 1.

$$\begin{cases} \psi_{ext,\alpha} = \psi_{ext} \cos\theta_e \\ \psi_{ext,\beta} = \psi_{ext} \sin\theta_e \end{cases} \tag{12}$$

Using (12), converting (10) into the α–β reference frame, the stator flux can be derived from the active flux [25]

$$\begin{cases} \psi_\alpha = \psi_{ext,\alpha} + L_q i_\alpha \\ \psi_\beta = \psi_{ext,\beta} + L_q i_\beta \end{cases} \tag{13}$$

2.4 *Unified PMSM model*

Substituting (13) into (1), the stator voltage equation of the IPMSM in the α–β reference frame can now be expressed as follows:

$$\begin{cases} u_\alpha = R_s i_\alpha + L_q \dfrac{di_\alpha}{dt} + \dfrac{d\psi_{ext,\alpha}}{dt} \\ u_\beta = R_s i_\beta + L_q \dfrac{di_\beta}{dt} + \dfrac{d\psi_{ext,\beta}}{dt} \end{cases} \tag{14}$$

Since the time constant of the mechanical system is much larger than that of the electrical system in the PMSM, the following

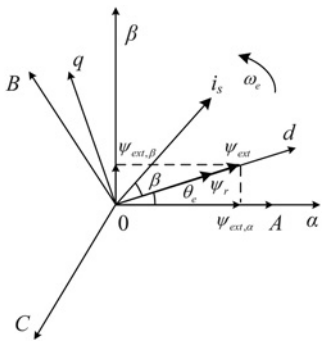

Fig. 1 *Active flux in coordinate frame*

doi: 10.1049/joe.2017.0160

equation can be derived:

$$\begin{cases} \dfrac{\mathrm{d}\psi_{\mathrm{ext},\alpha}}{\mathrm{d}t} = -\omega_{\mathrm{e}}\psi_{\mathrm{ext},\beta} \\ \dfrac{\mathrm{d}\psi_{\mathrm{ext},\beta}}{\mathrm{d}t} = \omega_{\mathrm{e}}\psi_{\mathrm{ext},\alpha} \end{cases} \tag{15}$$

The equations for an IPMSM in the α–β reference frame can be expressed as follows:

$$\begin{cases} \dfrac{\mathrm{d}i_\alpha}{\mathrm{d}t} = -\dfrac{R_{\mathrm{s}}}{L_q}i_\alpha + \dfrac{u_\alpha}{L_q} + \dfrac{\omega_{\mathrm{e}}}{L_q}\psi_{\mathrm{ext},\beta} \\ \dfrac{\mathrm{d}i_\beta}{\mathrm{d}t} = -\dfrac{R_{\mathrm{s}}}{L_q}i_\beta + \dfrac{u_\beta}{L_q} - \dfrac{\omega_{\mathrm{e}}}{L_q}\psi_{\mathrm{ext},\alpha} \end{cases} \tag{16}$$

Remark 1: It is evident that (16) of the IPMSM by active flux is equivalent to (3) of the SPMSM in the α–β axis reference frame. This results in a reduction in the dependence on the d-axis inductance and thus eliminating the salient pole for IPMSM. The advantages of this model include simple and generic equations with only two required parameters L_q and R_{s}.

The 'active flux' concept can turn all rotor salient-pole ac machines into fictitious rotor non-salient-pole machines [24–29].

3 Sensorless control of IPMSM by a variable gain adaptive SMO

In this section, a variable gain adaptive SMO for PMSM sensorless control is designed to estimate the rotor speed and the stator resistance in the d–q reference frame. Then, the estimated values are inputted to the active flux SMO.

3.1 Design the variable gain adaptive SMO

According to (6), the mathematical model for the IPMSM can be expressed as follows:

$$\begin{cases} \dot{\boldsymbol{x}} = \boldsymbol{A}\boldsymbol{x} + \boldsymbol{B}\boldsymbol{u} + \boldsymbol{D} \\ \boldsymbol{y} = \boldsymbol{C}\boldsymbol{x} \end{cases} \tag{17}$$

where

$$\boldsymbol{A} = \begin{bmatrix} -\dfrac{R_{\mathrm{s}}}{L_d} & \omega_{\mathrm{e}}\dfrac{L_q}{L_d} \\ -\omega_{\mathrm{e}}\dfrac{L_d}{L_q} & -\dfrac{R_{\mathrm{s}}}{L_q} \end{bmatrix}, \quad \boldsymbol{B} = \begin{bmatrix} \dfrac{1}{L_d} & 0 \\ 0 & \dfrac{1}{L_q} \end{bmatrix}$$

$$\boldsymbol{C} = \begin{bmatrix} 1 & 0 \\ 0 & 1 \end{bmatrix}, \quad \boldsymbol{D} = \begin{bmatrix} 0 & -\omega_{\mathrm{e}}\dfrac{\psi_{\mathrm{r}}}{L_q} \end{bmatrix}^{\mathrm{T}}$$

$$\boldsymbol{x} = \begin{bmatrix} i_d & i_q \end{bmatrix}^{\mathrm{T}}, \quad \boldsymbol{u} = \begin{bmatrix} u_d & u_q \end{bmatrix}^{\mathrm{T}}$$

Define the stators current errors

$$\boldsymbol{e} = \begin{bmatrix} e_d & e_q \end{bmatrix}^{\mathrm{T}} = \boldsymbol{x} - \hat{\boldsymbol{x}} = \begin{bmatrix} \bar{i}_d & \bar{i}_q \end{bmatrix}^{\mathrm{T}} \tag{18}$$

where $\bar{i}_d = i_d - \hat{i}_d$, $\bar{i}_q = i_q - \hat{i}_q$.

The proposed variable gain adaptive SMO can be designed as follows in order to estimate both the speed and stator resistance:

$$\dot{\hat{\boldsymbol{x}}} = \hat{\boldsymbol{A}}\hat{\boldsymbol{x}} + \boldsymbol{B}\boldsymbol{u} + \hat{\boldsymbol{D}} + \boldsymbol{v} \tag{19}$$

where

$$\hat{\boldsymbol{A}} = \begin{bmatrix} -\dfrac{\hat{R}_{\mathrm{s}}}{L_d} & \hat{\omega}_{\mathrm{e}}\dfrac{L_q}{L_d} \\ -\hat{\omega}_{\mathrm{e}}\dfrac{L_d}{L_q} & -\dfrac{\hat{R}_{\mathrm{s}}}{L_q} \end{bmatrix}, \quad \hat{\boldsymbol{D}} = \begin{bmatrix} 0 \\ -\hat{\omega}_{\mathrm{e}}\dfrac{\psi_{\mathrm{r}}}{L_q} \end{bmatrix}, \quad \hat{\boldsymbol{x}} = \begin{bmatrix} \hat{i}_d & \hat{i}_q \end{bmatrix}^{\mathrm{T}}$$

'^' denotes the estimated values. $\boldsymbol{v} = \boldsymbol{K}_1\|\boldsymbol{e}\|\mathrm{sign}(\boldsymbol{e})$, $\boldsymbol{K}_1 = k_1\boldsymbol{I}$, $k_1 > 0$, $\boldsymbol{I} = \begin{bmatrix} 1 & 0 \\ 0 & 1 \end{bmatrix}$, $\boldsymbol{K}_1\|\boldsymbol{e}\|$ is the sliding switch gain.

Remark 2: The sliding switch gain $\boldsymbol{K}_1\|\boldsymbol{e}\|$ varies according to the stators current errors, which effectively reduces the chattering phenomenon.

Then, the error dynamics equation is obtained by subtracting (19) from (17)

$$\dot{\boldsymbol{e}} = \boldsymbol{A}\boldsymbol{e} + \bar{\boldsymbol{A}}\hat{\boldsymbol{x}} + \bar{\boldsymbol{D}} - \boldsymbol{v} \tag{20}$$

where

$$\bar{\boldsymbol{A}} = \boldsymbol{A} - \hat{\boldsymbol{A}} = \begin{bmatrix} -\dfrac{\bar{R}_{\mathrm{s}}}{L_d} & \bar{\omega}_{\mathrm{e}}\dfrac{L_q}{L_d} \\ -\bar{\omega}_{\mathrm{e}}\dfrac{L_d}{L_q} & -\dfrac{\bar{R}_{\mathrm{s}}}{L_q} \end{bmatrix},$$

$$\bar{\boldsymbol{D}} = \boldsymbol{D} - \hat{\boldsymbol{D}} = \begin{bmatrix} 0 & -\bar{\omega}_{\mathrm{e}}\dfrac{\psi_{\mathrm{r}}}{L_q} \end{bmatrix}^{\mathrm{T}}$$

$\bar{R}_{\mathrm{s}} = R_{\mathrm{s}} - \hat{R}_{\mathrm{s}}$, $\bar{\omega}_{\mathrm{e}} = \omega_{\mathrm{e}} - \hat{\omega}_{\mathrm{e}}$.

Based on the sliding-mode control theory, the sliding mode manifold is defined upon the stator current errors

$$\boldsymbol{s} = \begin{bmatrix} s_1 & s_2 \end{bmatrix}^{\mathrm{T}} = \boldsymbol{e} = \begin{bmatrix} e_d & e_q \end{bmatrix}^{\mathrm{T}} \tag{21}$$

3.2 Lyapunov stability analysis, estimation of speed and position

Theorem 1: The stator current error system (20) converge to zero exponentially, if the sliding mode manifold is chosen as (21), and $k_1 \geq (L\|\omega_{\mathrm{e}}\|/2) - (R_{\mathrm{s}}/L_d) + \eta$, $\eta > 0$, $L = (L_q/L_d) - (L_d/L_q) > 0$. Then, the stator resistance estimation can be derived as [10]

$$\hat{R}_{\mathrm{s}} = l_R\int\left(-\frac{1}{L_d}\bar{i}_d\hat{i}_d - \frac{1}{L_q}\bar{i}_q\hat{i}_q\right)\mathrm{d}t \tag{22}$$

Moreover, the electrical angular velocity can be derived as

$$\hat{\omega}_{\mathrm{e}} = l_\omega\int\left(\frac{L_q}{L_d}\bar{i}_d\hat{i}_q - \frac{L_d}{L_q}\bar{i}_q\hat{i}_d - \bar{i}_q\frac{\psi_{\mathrm{r}}}{L_q}\right)\mathrm{d}t \tag{23}$$

Proof: The Lyapunov function is selected as

$$V = \frac{1}{2}\left(\boldsymbol{e}^{\mathrm{T}}\boldsymbol{e} + \frac{\bar{R}_{\mathrm{s}}^2}{l_R} + \frac{\bar{\omega}_{\mathrm{e}}^2}{l_\omega}\right) \tag{24}$$

where l_R, l_ω are positive constants.

Assuming that changes in the stator resistance R_s and the electrical angular velocity ω_e occur slowly, it can be assumed that R_s and ω_e remain approximately constant within a given sampling interval.

Differentiating (24) with respect to time and substituting (20) into it, then the following equation is obtained:

$$\begin{aligned}\dot{V} &= \boldsymbol{e}^{\mathrm{T}}\dot{\boldsymbol{e}} - \frac{\dot{\bar{R}}_s\bar{R}_s}{l_R} - \frac{\bar{\omega}_e\dot{\bar{\omega}}_e}{l_\omega} \\ &= \boldsymbol{e}^{\mathrm{T}}\boldsymbol{A}\boldsymbol{e} + \boldsymbol{e}^{\mathrm{T}}\boldsymbol{A}\bar{\hat{\boldsymbol{x}}} + \boldsymbol{e}^{\mathrm{T}}\bar{\boldsymbol{D}} - \boldsymbol{e}^{\mathrm{T}}\boldsymbol{v} - \frac{\dot{\bar{R}}_s\bar{R}_s}{l_R} - \frac{\bar{\omega}_e\dot{\bar{\omega}}_e}{l_\omega} \\ &= \boldsymbol{e}^{\mathrm{T}}\boldsymbol{A}\boldsymbol{e} - \boldsymbol{e}^{\mathrm{T}}\boldsymbol{v} - \bar{R}_s\left(\frac{1}{L_d}\bar{i}_d\hat{i}_d + \frac{1}{L_q}\bar{i}_q\hat{i}_q + \frac{\dot{\bar{R}}_s}{l_R}\right) \\ &\quad + \bar{\omega}_e\left(\frac{L_q}{L_d}\bar{i}_d\hat{i}_q - \frac{L_d}{L_q}\bar{i}_q\hat{i}_d - \bar{i}_q\frac{\psi_r}{L_q} - \frac{\dot{\bar{\omega}}_e}{l_\omega}\right)\end{aligned} \tag{25}$$

In order to drive the system to be convergent, i.e. let

$$\boldsymbol{e}^{\mathrm{T}}\boldsymbol{A}\boldsymbol{e} - \boldsymbol{e}^{\mathrm{T}}\boldsymbol{v} < 0 \tag{26}$$

$$\bar{R}_s\left(\frac{1}{L_d}\bar{i}_d\hat{i}_d + \frac{1}{L_q}\bar{i}_q\hat{i}_q + \frac{\dot{\bar{R}}_s}{l_R}\right) = 0 \tag{27}$$

$$\bar{\omega}_e\left(\frac{L_q}{L_d}\bar{i}_d\hat{i}_q - \frac{L_d}{L_q}\bar{i}_q\hat{i}_d - \bar{i}_q\frac{\psi_r}{L_q} - \frac{\dot{\bar{\omega}}_e}{l_\omega}\right) = 0 \tag{28}$$

Since $L_d < L_q$, the condition (26) is described as follows:

$$\begin{aligned}\boldsymbol{e}^{\mathrm{T}}\boldsymbol{A}\boldsymbol{e} - \boldsymbol{e}^{\mathrm{T}}\boldsymbol{v} &\le -\frac{R_s}{L_d}e_d^2 - \frac{R_s}{L_d}e_q^2 + \omega_e\left(\frac{L_q}{L_d} - \frac{L_d}{L_q}\right)e_de_q \\ &\quad - k_1e_d^2\mathrm{sign}(e_d) - k_1e_q^2\mathrm{sign}(e_q) \\ &\le -\frac{R_s}{L_d}\|e_d\|^2 - \frac{R_s}{L_d}\|e_q\|^2 + \frac{L\|\omega_e\|}{2}\|e_d\|^2 \\ &\quad + \frac{L\|\omega_e\|}{2}\|e_q\|^2 - k_1\|e_d\|^2 - k_1\|e_q\|^2 \\ &= -\left(\frac{R_s}{L_d} - \frac{L\|\omega_e\|}{2} + k_1\right)\|\boldsymbol{e}\|^2 \\ &\le -\eta\|\boldsymbol{e}\|^2\end{aligned} \tag{29}$$

where $k_1 \ge (L\|\omega_e\|/2) - (R_s/L_d) + \eta$, $\eta > 0$, $L = (L_q/L_d) - (L_d/L_q) > 0$.

Combining (27)–(29) will yield $\dot{V} \le -\eta\|\boldsymbol{e}\|^2$. According to the Lyapunov stability theory, designed observer is stable. Therefore, k_1, which is large enough, can ensure both the existence of sliding motion and the asymptotical stability of sliding motion in the global scope.

From (27), the estimation of stator resistance may be derived as (22). Also, from (28), the electrical angular velocity may be derived as (23).

This completes the proof. □

4 Design SMO of active flux for IPMSM

In this section, the SMO of active flux for IPMSM is designed to estimate the active flux in the α–β reference frame. Then, the estimated torque could be derived based on the active flux and stator current.

4.1 Design the SMO of active flux

According to (16), the mathematical model for the IPMSM can be shown as follows:

$$\begin{cases}\dot{\boldsymbol{x}}' = \boldsymbol{A}'\boldsymbol{x} + \boldsymbol{B}'\boldsymbol{u}' + \boldsymbol{E}\boldsymbol{d} \\ \boldsymbol{y}' = \boldsymbol{C}\boldsymbol{x}'\end{cases} \tag{30}$$

where

$$\begin{aligned}&\boldsymbol{x}' = \begin{bmatrix} i_\alpha & i_\beta \end{bmatrix}^{\mathrm{T}}, \quad \boldsymbol{u}' = \begin{bmatrix} u_\alpha & u_\beta \end{bmatrix}^{\mathrm{T}}, \quad d = \begin{bmatrix} \psi_{\mathrm{ext},\alpha} & \psi_{\mathrm{ext},\beta} \end{bmatrix}^{\mathrm{T}} \\ &\boldsymbol{A}' = -(R_s/L_q)\boldsymbol{I}, \quad \boldsymbol{B}' = (1/L_q)\boldsymbol{I}, \quad \boldsymbol{E} = -(\omega_e/L_q)\boldsymbol{J} \\ &\boldsymbol{C} = \boldsymbol{I}, \quad \boldsymbol{I} = \begin{bmatrix} 1 & 0 \\ 0 & 1 \end{bmatrix}, \quad \boldsymbol{J} = \begin{bmatrix} 0 & -1 \\ 1 & 0 \end{bmatrix}\end{aligned}$$

The stators current errors are defined as

$$\boldsymbol{e}' = \begin{bmatrix} e_a & e_\beta \end{bmatrix}^{\mathrm{T}} = \boldsymbol{x}' - \hat{\boldsymbol{x}}' = \begin{bmatrix} \bar{i}_\alpha & \bar{i}_\beta \end{bmatrix}^{\mathrm{T}} \tag{31}$$

where $\bar{i}_\alpha = i_\alpha - \hat{i}_\alpha$, $\bar{i}_\beta = i_\beta - \hat{i}_\beta$.

Using the IPMSM model (30) in the α–β reference frame, the SMO can be designed as follows:

$$\dot{\hat{\boldsymbol{x}}}' = \boldsymbol{A}'\hat{\boldsymbol{x}}' + \boldsymbol{B}'\boldsymbol{u}' + \boldsymbol{v}' \tag{32}$$

where $\hat{\boldsymbol{x}}' = \begin{bmatrix} \hat{i}_\alpha & \hat{i}_\beta \end{bmatrix}^{\mathrm{T}}$, $\boldsymbol{v}' = \boldsymbol{K}_2\boldsymbol{H}(\boldsymbol{e}')$, $\boldsymbol{K}_2 = k_2\boldsymbol{I}$, $k_2 > 0$. '^' denotes the estimated values. k_2 is a sliding switch gain.

The switching function $\boldsymbol{H}(\boldsymbol{e}')$ is defined by the following sigmoid function [31]:

$$\boldsymbol{H}(\boldsymbol{e}') = \frac{2}{1 + \mathrm{e}^{-a\boldsymbol{e}'}} - 1 \tag{33}$$

where a is a positive constant that can be adjusted the slope of the sigmoid function. The discontinuous sign function is replaced by a continuous sigmoid function, which effectively reduces the chattering phenomenon.

Hence, the error dynamics equation can be obtained by subtracting (32) from (30) as

$$\dot{\boldsymbol{e}}' = \boldsymbol{A}'\boldsymbol{e}' + \boldsymbol{E}\boldsymbol{d} - \boldsymbol{v}' \tag{34}$$

The sliding mode manifold is defined upon the stator current errors $\boldsymbol{s}' = \boldsymbol{e}'$.

4.2 Lyapunov stability analysis

Theorem 2: The stator current error system (34) converge to zero exponentially, if the sliding mode manifold is chosen as $\boldsymbol{s}' = \boldsymbol{e}'$, and $k_2 > \max\{-\|\dot{\psi}_{\mathrm{ext},\beta}\|/L_q, -\|\dot{\psi}_{\mathrm{ext},\alpha}\|/L_q\}$.

Proof: The Lyapunov function is selected as

$$V' = \frac{1}{2}\boldsymbol{e}'^{\mathrm{T}}\boldsymbol{e}' \tag{35}$$

Then differentiating (35) with respect to time and substituting (34) into it, then the following equation is obtained:

$$\dot{V}' = \boldsymbol{e}'^{\mathrm{T}}\dot{\boldsymbol{e}}' = \boldsymbol{e}'^{\mathrm{T}}\boldsymbol{A}'\boldsymbol{e}' + \boldsymbol{e}'^{\mathrm{T}}\boldsymbol{E}\boldsymbol{d} - \boldsymbol{e}'^{\mathrm{T}}\boldsymbol{v}' \tag{36}$$

where

$$\boldsymbol{e}'^{\mathrm{T}}\boldsymbol{A}'\boldsymbol{e}' = -\frac{R_\mathrm{s}}{L_q}e_\alpha^2 - \frac{R_\mathrm{s}}{L_q}e_\beta^2 \tag{37}$$

$$\boldsymbol{e}'^{\mathrm{T}}\boldsymbol{E}\boldsymbol{d} = \frac{e_\alpha}{L_q}\omega_\mathrm{e}\psi_{\mathrm{ext},\beta} - \frac{e_\beta}{L_q}\omega_\mathrm{e}\psi_{\mathrm{ext},\alpha} = -\frac{e_\alpha}{L_q}\dot{\psi}_{\mathrm{ext},\alpha} - \frac{e_\beta}{L_q}\dot{\psi}_{\mathrm{ext},\beta} \tag{38}$$

Substituting (37) and (38) into (36), then following equation is obtained:

$$\begin{aligned}
\dot{V}' &= -\frac{R_\mathrm{s}}{L_q}(e_\alpha^2 + e_\beta^2) - \frac{e_\alpha}{L_q}\dot{\psi}_{\mathrm{ext},\alpha} - \frac{e_\beta}{L_q}\dot{\psi}_{\mathrm{ext},\beta} - e_\alpha k_2 H(e_\alpha) - e_\beta k_2 H(e_\beta) \\
&= -\frac{R_\mathrm{s}}{L_q}\left(e_\alpha^2 + e_\beta^2\right) - e_\alpha\left(\frac{\dot{\psi}_{\mathrm{ext},\alpha}}{L_q} + k_2 H(e_\alpha)\right) - e_\beta\left(\frac{\dot{\psi}_{\mathrm{ext},\beta}}{L_q} + k_2 H(e_\beta)\right) \\
&\le -\frac{R_\mathrm{s}}{L_q}\|\boldsymbol{e}'\|^2 - \frac{\|e_\alpha\|}{L_q}\left\|\dot{\psi}_{\mathrm{ext},\alpha}\right\| - \frac{\|e_\beta\|}{L_q}\left\|\dot{\psi}_{\mathrm{ext},\beta}\right\| - k_2\|e_\alpha\| - k_2\|e_\beta\| \\
&\le -\frac{R_\mathrm{s}}{L_q}\|\boldsymbol{e}'\|^2 - \|e_\alpha\|\left(\frac{1}{L_q}\left\|\dot{\psi}_{\mathrm{ext},\alpha}\right\| + k_2\right) - \|e_\beta\|\left(\frac{1}{L_q}\left\|\dot{\psi}_{\mathrm{ext},\beta}\right\| + k_2\right)
\end{aligned} \tag{39}$$

Chosen $k_2 > \max\{-\left\|\dot{\psi}_{\mathrm{ext},\beta}\right\|/L_q, -\left\|\dot{\psi}_{\mathrm{ext},\alpha}\right\|/L_q\}$, then will yield $\dot{V}' \le -(R_\mathrm{s}/L_q)\|\boldsymbol{e}'\|^2$. According to the Lyapunov stability theory, the designed observer is stable. Therefore, k_2, which is large enough, can ensure both the existence of sliding motion and the asymptotical stability of sliding motion in the global scope.

This completes the proof. □

4.3 Estimate the active flux and torque

Once the system reaches the sliding manifold, according to the sliding mode equivalent principle [32], the following equation is obtained:

$$\boldsymbol{s}' = \dot{\boldsymbol{s}}' = \boldsymbol{e}' = \dot{\boldsymbol{e}}' = 0 \tag{40}$$

Substituting (40) into (34) yields

$$\boldsymbol{E}\boldsymbol{d} = \boldsymbol{v}' \tag{41}$$

The estimated active flux is derived as follows:

$$\begin{cases} \hat{\psi}_{\mathrm{ext},\beta} &= L_q v_\alpha/\omega_\mathrm{e} \\ \hat{\psi}_{\mathrm{ext},\alpha} &= -L_q v_\beta/\omega_\mathrm{e} \end{cases} \tag{42}$$

The estimated active flux amplitude $\hat{\psi}_{\mathrm{ext}}$ can then be estimated

$$\hat{\psi}_{\mathrm{ext}} = \sqrt{\hat{\psi}_{\mathrm{ext},\alpha}^2 + \hat{\psi}_{\mathrm{ext},\beta}^2} \tag{43}$$

The current $\hat{i}_d$, $\hat{i}_q$ can be estimated using Park transformation of the estimated current $\hat{i}_\alpha$, $\hat{i}_\beta$ by the SMO of active flux (32).

Substituting the estimated amplitude of the active flux $\hat{\psi}_{\mathrm{ext}}$ and stator current $\hat{i}_q$ into (9) yields the estimated torque

$$\hat{T}_\mathrm{e} = \frac{3}{2}n_\mathrm{p}\hat{\psi}_{\mathrm{ext}}\hat{i}_q \tag{44}$$

Remark 3: Based on the above analysis, the procedure of the proposed scheme is summarised as follows:

(i) *Step 1:* The electrical angular velocity $\hat{\omega}_\mathrm{e}$ is estimated using (23), and the stator resistance $\hat{R}_\mathrm{s}$ is estimated using (22) by the variable gain adaptive SMO exploiting the stator currents i_d, i_q and voltages u_d, u_q. The rotor electrical angle $\hat{\theta}_\mathrm{e}$ was derived through the integration of the rotor electrical angular velocity $\hat{\omega}_\mathrm{e}$.

(ii) *Step 2:* The active flux $\hat{\psi}_{\mathrm{ext},\alpha}$, $\hat{\psi}_{\mathrm{ext},\beta}$ is estimated using (42) by the SMO of active flux exploiting the stator current i_α, i_β, voltage u_α, u_β and the estimated electrical angular velocity $\hat{\omega}_\mathrm{e}$, the estimated stator resistance $\hat{R}_\mathrm{s}$.

(iii) *Step 3:* The estimated active flux amplitude $\hat{\psi}_{\mathrm{ext}}$ was derived using (43). The estimated current $\hat{i}_q$ was derived through the Park transformation of the estimated stator current $\hat{i}_\alpha$, $\hat{i}_\beta$ by the active flux observer (32). The estimated torque could then be calculated by (44). The torque-sensorless closed-loop control system is constituted.

5 Simulations and experiments

To check the performance of the proposed scheme, simulations are carried out on Matlab/Simulink, and experiments are carried out on the RT-LAB platform. The block diagram of the IPMSM torque-sensorless closed-loop control system is presented in Fig. 2. The MTPA [10] control scheme is carried out on an IPMSM.

The IPMSM parameters are listed in Table 1.

The parameters of the variable gain adaptive SMO are set as follows: $k_1 = 300$, $l_R = 0.1$, $l_\omega = 50$. The parameters of the SMO of active flux are set as $k_2 = 6000$, $a = 1$. The same parameters are used both in simulation and experiments.

5.1 Simulation results

In order to investigate the dynamic performance of the proposed torque-sensorless closed-loop control system, the initial rotor electrical angular velocity is set to 50 rad/s and subsequently increases to 200 rad/s at 0.2 s; the initial stator resistance is set to 0.02 Ω and subsequently increases to 0.04 Ω at 0.4 s; the initial load torque is set to 500 Nm and subsequently increases to 1000 Nm at 0.6 s.

Figs. 3–6 demonstrate the performance of the proposed variable gain adaptive SMO for IPMSM sensorless control. The estimated d–q axis stator currents $\hat{i}_d$, $\hat{i}_q$ are shown in Fig. 3. It is shown that the estimated q-axis stator current $\hat{i}_q$ is increased when the torque command is increased from 500 to 1000 Nm at 0.6 s. The actual stator resistance R_s, the estimated stator resistance $\hat{R}_\mathrm{s}$ and the error of stator resistance ΔR_s are shown in Fig. 4. The actual electrical angular velocity ω_e, the estimated electrical angular velocity $\hat{\omega}_\mathrm{e}$ and the error $\Delta\omega_\mathrm{e}$ are given in Fig. 5. The actual electrical position θ_e, the estimated electrical position $\hat{\theta}_\mathrm{e}$ and the errors $\Delta\theta_\mathrm{e}$ are given in Fig. 6. Figs. 4–6 show that the increase of the electrical angular velocity has an impact on the estimated stator resistance $\hat{R}_\mathrm{s}$, the estimated electrical angular velocity $\hat{\omega}_\mathrm{e}$ and the estimated electrical position $\hat{\theta}_\mathrm{e}$ at 0.2 s. However, they converge to the actual value quickly, which verifies the robustness of the proposed approach.

Figs. 7–10 demonstrate the performance of IPMSM by the proposed active flux SMO. The estimated stator currents $\hat{i}_\alpha$, $\hat{i}_\beta$ are shown in Fig. 7. The estimated $\hat{\psi}_{\mathrm{ext},\alpha}$, $\hat{\psi}_{\mathrm{ext},\beta}$ and the amplitude of active flux $\hat{\psi}_{\mathrm{ext}}$ are shown in Fig. 8. The trace of the active flux is shown in Fig. 9. The given torque T_e^*, the estimated torque $\hat{T}_\mathrm{e}$ and errors ΔT_e are shown in Fig. 10.

It can be drawn from the simulation results:

(i) Before 0.2 s, the frequency of the stator current and active flux is low. After 0.2 s, the frequency of the stator current and active flux increases when the electrical angular velocity increases to 200 rad/s.

(ii) Before 0.6 s, the stator current amplitude is small because the torque command is 500 Nm. After 0.6 s, the torque command

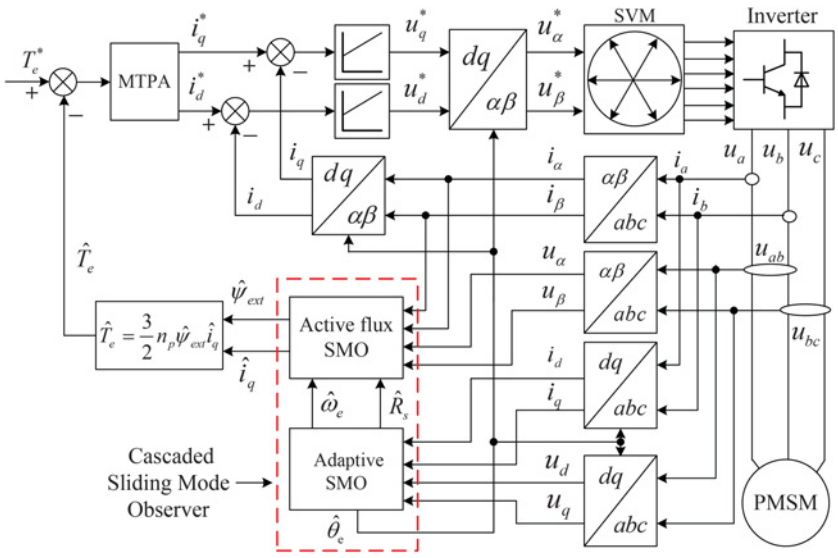

Fig. 2 *Schematic diagram of IPMSM torque-sensorless closed-loop control system*

Table 1 Parameters of IPMSM

Parameters	Unit	Values
rated voltage (U_N)	V	1500
rated current (I_N)	A	400
rated speed (ω_e)	rad/s	800
stator resistance (R_s)	Ω	0.02
q-axis inductance (L_q)	H	0.003572
d-axis inductance (L_d)	H	0.002
rotational inertia (J)	kg · m^2	100
rotor PM flux (ψ_r)	Wb	0.892
number of pole pairs (n_p)	pairs	4

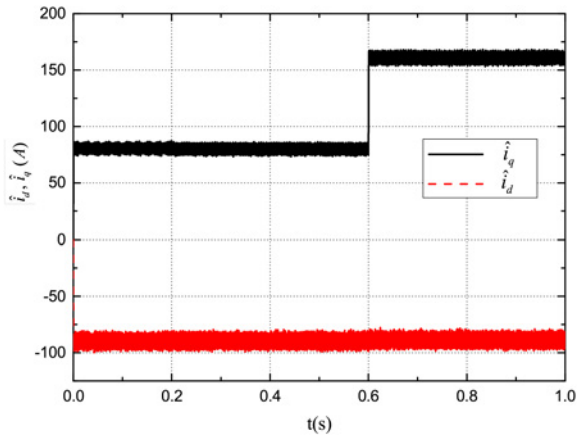

Fig. 3 *Estimated stator currents* $\hat{i}_d$, $\hat{i}_q$

increases to 1000 Nm resulting in increase of the stator current amplitude.

(iii) When the motor starts or the speed changes, the stator current, the active flux and the torque fluctuate, but they converge to the actual value quickly.

5.2 Experiments results

RT-LAB is a powerful, modular, distributed, real-time platform from OPAL-RT Technologies, Inc. It supports model-based design using rapid control prototyping and hardware-in-the-loop simulation (HILS) of complex dynamic systems [33].

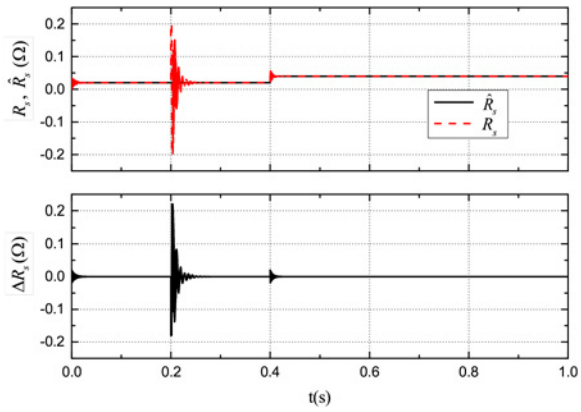

Fig. 4 *Actual, estimated stator resistances* R_s, $\hat{R}_s$ *and the error* ΔR_s

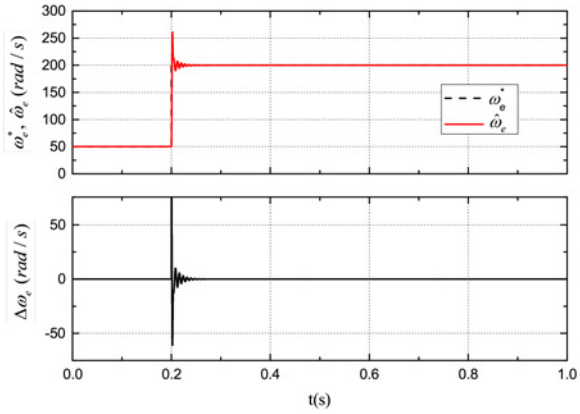

Fig. 5 *Actual, estimated electrical angular velocities* ω_e, $\hat{\omega}_e$ *and the errors* $\Delta\omega_e$

To implement the proposed scheme, HILS experiments are carried out on an OP5600 RT-Lab platform. The RT-Lab platform is shown in Fig. 11, and the configuration is shown in Fig. 12. The controller is a TMS320F2812 digital signal processor, which implements high-performance control and computation. The PWM switching frequency is chosen as 5 kHz. The sampling period is chosen as 20 μs.

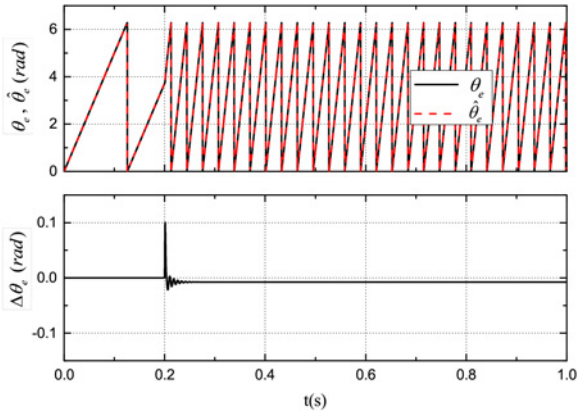

Fig. 6 *Actual, estimated electrical positions θ_e, $\hat{\theta}_e$ and the errors $\Delta\theta_e$*

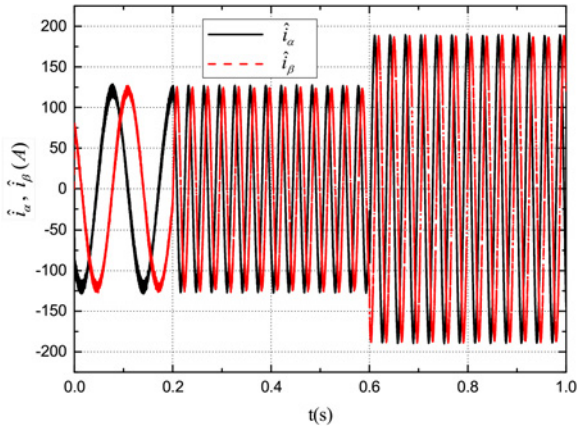

Fig. 7 *Estimated stator currents $\hat{i}_\alpha$, $\hat{i}_\beta$*

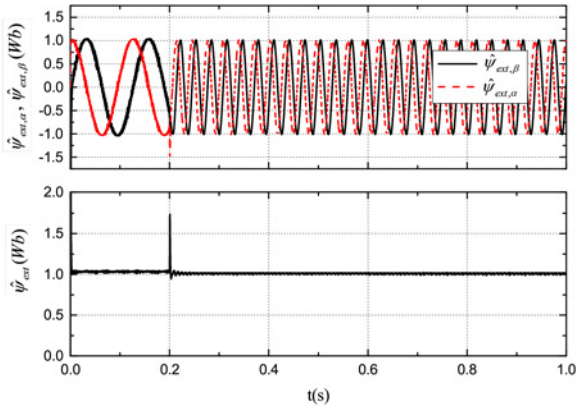

Fig. 8 *Estimated active fluxes $\hat{\psi}_{ext,\alpha}$, $\hat{\psi}_{ext,\beta}$, and the amplitude $\hat{\psi}_{ext}$*

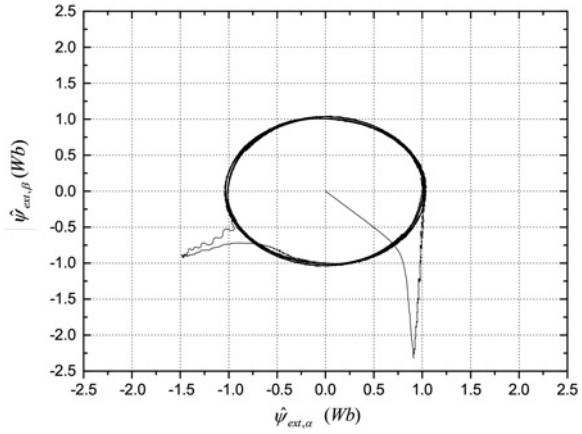

Fig. 9 *Observed trace of active flux*

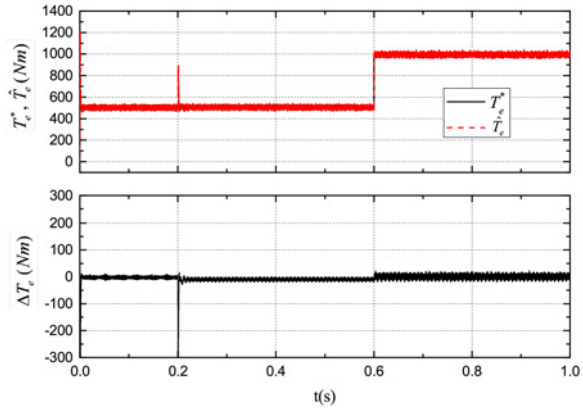

Fig. 10 *Given, estimated torques T_e^*, $\hat{T}_e$ and the errors ΔT_e*

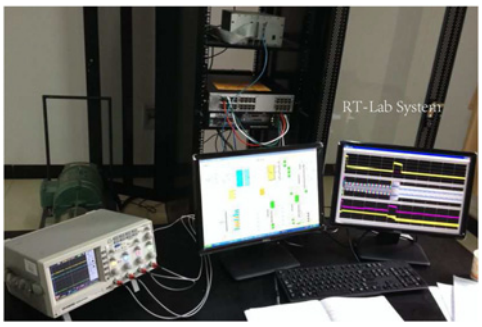

Fig. 11 *RT-Lab platform*

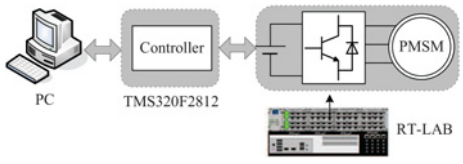

Fig. 12 *Configuration of the RT-LAB HILS system*

Figs. 13 and 14 demonstrate the performance of the IPMSM sensorless control by the proposed variable gain adaptive SMO. Fig. 13 shows the waveform of the actual stator resistance R_s, the estimated stator resistance $\hat{R}_s$ and the estimated stator currents $\hat{i}_d$, $\hat{i}_q$. Fig. 13*a* shows the waveform when the electrical angular velocity increase from 50 to 200 rad/s. It is evident that the estimated stator resistance $\hat{R}_s$ has fluctuation. Fig. 13*b* shows the waveform when the stator resistance increase from 0.02 to 0.04 Ω. It is evident that the estimated stator resistance $\hat{R}_s$ can rapidly track the actual stator resistance R_s. Fig. 14 shows that the actual and estimated electrical angular velocities ω_e, $\hat{\omega}_e$, respectively, the actual and estimated electrical positions θ_e, $\hat{\theta}_e$, respectively. It is evident that the estimated electrical angular velocity and position can also rapidly track the actual speed value.

Figs. 15 and 16 demonstrate the effectiveness of the torque control for IPMSM by proposed active flux SMO. Fig. 15 shows that the estimated active flux $\hat{\psi}_{ext,\alpha}$, $\hat{\psi}_{ext,\beta}$, and the amplitude of active flux $\hat{\psi}_{ext}$. Note that the actual active flux is unavailable and

doi: 10.1049/joe.2017.0160

the calculated active flux is determined by (42) and (43) using the estimated electrical angular velocity $\hat{\omega}_e$. Fig. 16 shows the estimated stator currents $\hat{i}_\alpha$, $\hat{i}_\beta$ and the given torque T_e^*, the estimated torque $\hat{T}_e$. Fig. 16*a* shows the waveform when the electrical angular velocity increase from 50 to 200 rad/s and torque is 500 Nm. Fig. 16*b* shows the waveform when the torque increase from 500 to 1000 Nm. It is evident that the estimated torque value $\hat{T}_e$ can rapidly track the given torque value T_e^*.

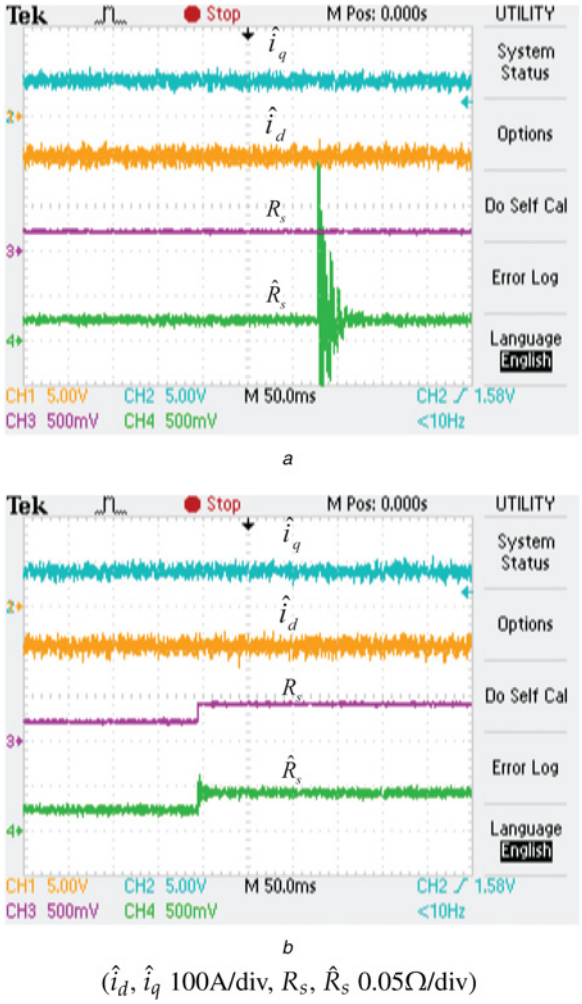

Fig. 13 *Experimental results: The estimated stator currents $\hat{i}_d$, $\hat{i}_q$ and the actual, estimated stator resistances R_s, $\hat{R}_s$*
a Electrical angular velocity increases from 50 to 200 rad/s
b Stator resistance increases from 0.02 to 0.04 Ω

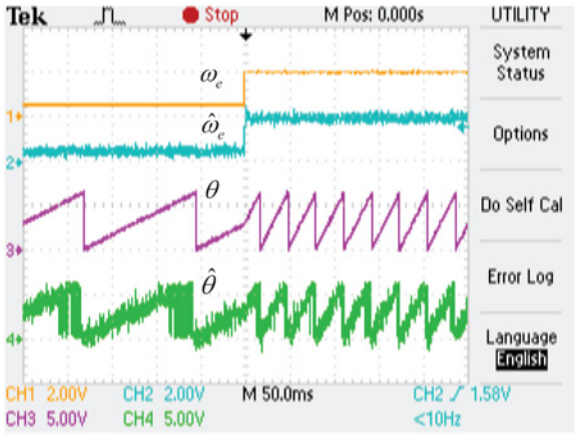

Fig. 14 *Experimental results. The actual and estimated rotor electrical angular velocities ω_e^* $\hat{\omega}_e$ and the actual and estimated rotor electrical positions θ_e, $\hat{\theta}_e$*

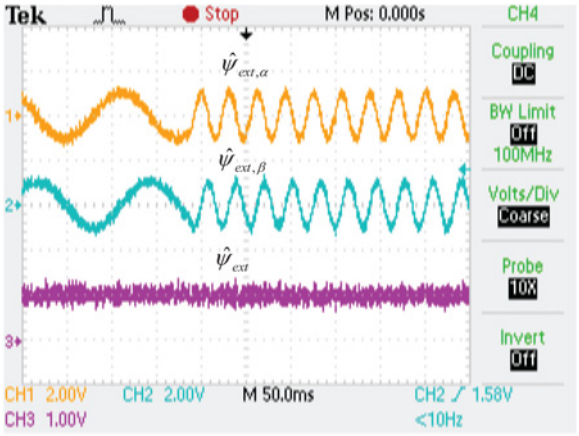

Fig. 15 *Experimental results. The estimated active fluxes $\hat{\psi}_{ext,\alpha}$, $\hat{\psi}_{ext,\beta}$, and the estimated amplitude of active flux $\hat{\psi}_{ext}$*

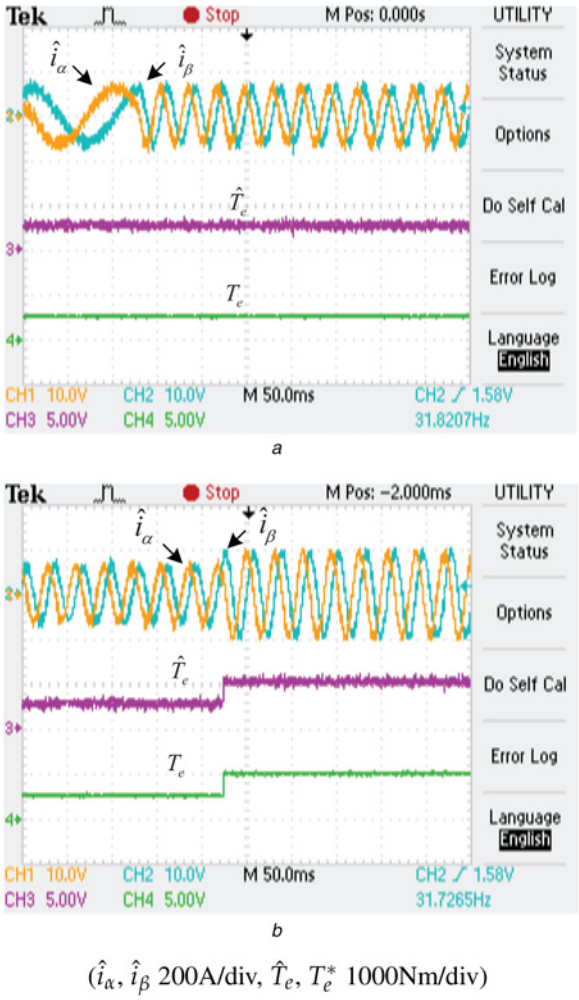

Fig. 16 *Experimental results: The estimated stator currents $\hat{i}_\alpha$, $\hat{i}_\beta$ and the given, estimated torque T_e^*, $\hat{T}_e$*
a Electrical angular velocity increases from 50 to 200 rad/s
b Torque increases from 500 to 1000 Nm

doi: 10.1049/joe.2017.0160

6 Conclusions

This paper designs the cascaded SMO for torque-sensorless closed-loop control method of IPMSM. A variable gain adaptive SMO is designed to achieve IPMSM sensorless control in a d–q reference frame, and another active flux SMO is designed to estimate both the active flux and the torque in the α–β reference frame. The performance of torque-sensorless control for IPMSM is achieved. The results of simulation and experimental validate the feasibility and effectiveness of the proposed approach. In the future, the cascaded non-singular fast terminal SMO will be designed for torque-sensorless closed-loop control of IPMSM, or the chattering elimination and the fast convergence of non-singular fast terminal-sliding-mode problem of IPMSM system will be considered.

7 Acknowledgments

This work was supported by the Natural Science Foundation of China under grant nos. 61473117 and 61503131, the Scientific Research Fund of the Hunan Provincial Education Department under grant nos. 16A058 and 17B073, the Hunan Provincial Natural Science Foundation of China under grant nos. 2017JJ4031 and 2016JJ5012, the Hunan Province Education Department under grant no. 13CY018, the Teaching Reform Fund of Hunan Province Education Department under grant no. Hunan Education Notice [2016] no. 400, the Teaching Reform of Degree and Postgraduate Education Fund of Hunan University of Technology under grant no. JG1604, the Key Laboratory for Electric Drive Control and Intelligent Equipment of Hunan Province Grant no. 2016TP1018, the Science and Technology Innovative Research Team in Higher Educational Institutions of Hunan Province.

8 References

[1] Jarzebowicz L., Karwowski K., Kulesza W.J.: 'Sensorless algorithm for sustaining controllability of IPMSM drive in electric vehicle after resolver fault', *Control Eng. Pract.*, 2017, **58**, pp. 117–126

[2] Preindl M., Bolognani S.: 'Optimal state reference computation with constrained MTPA criterion for PM motor drives', *IEEE Trans. Power Electron.*, 2015, **30**, pp. 4524–4535

[3] Zheng Z.D., Li Y.D., Xiao X., *ET AL.*: 'Load torque observer of permanent magnet synchronous motor', *Trans. Chin. Electrotech. Soc.*, 2010, **25**, pp. 30–36

[4] Zheng Z.D., Li Y.D., Fadel M., *ET AL.*: 'A rotor speed and load torque observer for PMSM based on extended Kalman filter'. IEEE Int. Conf. Industrial Technology, Bombay, India, 2006, pp. 1057–1062

[5] Zhu Y., Wu S.B., Wu Z.H., *ET AL.*: 'Precise torque control method of IPMSM in vehicle', *Trans. Chin. Soc. Agric. Mach.*, 2014, **45**, pp. 8–13

[6] Zhang C.F., He J., Jia L., *ET AL.*: 'Virtual line-shafting control for permanent magnet synchronous motor systems using sliding-mode observer', *IET Control Theory Appl.*, 2015, **9**, pp. 456–464

[7] Huang W.Q., Zhang Y.T., Zhang X.C., *ET AL.*: 'Accurate torque control of interior permanent magnet synchronous machine', *IEEE Trans. Energy Convers.*, 2014, **29**, pp. 29–37

[8] Kim S.I., Im J.H., Song E.Y., *ET AL.*: 'A new rotor position estimation method of IPMSM using all-pass filter on high-frequency rotating voltage signal injection', *IEEE Trans. Ind. Electron.*, 2016, **63**, pp. 6499–6509

[9] Wang G.L., Yang L., Zhang G.Q., *ET AL.*: 'Comparative investigation of pseudorandom high-frequency signal injection schemes for sensorless IPMSM drives', *IEEE Trans. Power Electron.*, 2017, **32**, pp. 2123–2132

[10] Foo G., Rahman M.F.: 'Sensorless sliding-mode MTPA control of an IPM synchronous motor drive using a sliding-mode observer and HF signal injection', *IEEE Trans. Ind. Electron.*, 2010, **57**, pp. 1270–1278

[11] Yang S.C., Hsu Y.L.: 'Full speed region sensorless drive of permanent-magnet machine combining saliency-based and back-EMF-based drive', *IEEE Trans. Ind. Electron.*, 2017, **64**, pp. 1092–1101

[12] Saadaoui O., Khlaief A., Abassi M., *ET AL.*: 'A sliding-mode observer for high-performance sensorless control of PMSM with initial rotor position detection', *Int. J. Control*, 2017, **90**, pp. 377–392

[13] Zhang X.G., Li Z.X.: 'Sliding-mode observer-based mechanical parameter estimation for permanent magnet synchronous motor', *IEEE Trans. Power Electron.*, 2016, **31**, pp. 5732–5745

[14] Song X., Fang J., Han B., *ET AL.*: 'Adaptive compensation method for high-speed surface PMSM sensorless drives of EMF-based position estimation error', *IEEE Trans. Power Electron.*, 2016, **31**, pp. 1438–1449

[15] Nguyen D., Dutta R., Rahman M.F., *ET AL.*: 'Performance of a sensorless controlled concentrated-wound interior permanent-magnet synchronous machine at low and zero speed', *IEEE Trans. Ind. Electron.*, 2016, **63**, pp. 2016–2026

[16] Comanescu M.: 'Sensorless rotor position estimation of PMSM by full-order and sliding mode EMF observers with speed estimate', *Int. J. Veh. Auton. Syst.*, 2013, **11**, pp. 157–189

[17] He J., Zhang C.F., Mao S., *ET AL.*: 'Demagnetization fault detection in permanent magnet synchronous motors based on sliding observer', *J. Nonlinear Sci. Appl.*, 2016, **9**, pp. 2039–2048

[18] Zhao K.H., Chen T.F., Zhang C.F., *ET AL.*: 'Online fault detection of permanent magnet demagnetization for IPMSMs by nonsingular fast terminal-sliding-mode observer', *Sensors*, 2014, **14**, pp. 23119–23136

[19] Huang G., Luo Y.P., Zhang C.F., *ET AL.*: 'Current sensor fault diagnosis based on a sliding mode observer for PMSM driven systems', *Sensors*, 2015, **15**, pp. 11027–11049

[20] Zhang C.F., Liao H.J., Li X.F., *ET AL.*: 'Fault reconstruction based on sliding mode observer for current sensors of PMSM', *J. Sens.*, 2016, **2016**, pp. 1–9

[21] Rubio J.J.: 'Hybrid controller with observer for the estimation and rejection of disturbances', *ISA Trans.*, 2016, **65**, pp. 445–455

[22] Rubio J. de Jesus: 'Sliding mode control of robotic arms with dead zone', *IET Control Theory Appl.*, 2017, **11**, pp. 1214–1221

[23] Aguilar-Ibanez C.: 'Stabilization of the PVTOL aircraft based on a sliding mode and a saturation function', *Int. J. Robust Nonlinear Control*, 2017, **27**, pp. 843–859

[24] Boldea I., Paicu M.C., Andreescu G.D., *ET AL.*: ''Active Flux' DTFC-SVM sensorless control of IPMSM', *IEEE Trans. Energy Convers.*, 2009, **24**, pp. 314–322

[25] Foo G., Rahman M.F.: 'Sensorless vector control of interior permanent magnet synchronous motor drives at very low speed without signal injection', *IET Electr. Power Appl.*, 2010, **4**, pp. 131–139

[26] Liu J.B., Nondahl T.A., Schmidt P.B., *ET AL.*: 'Rotor position estimation for synchronous machines based on equivalent EMF', *IEEE Trans. Ind. Appl.*, 2011, **47**, pp. 1310–1318

[27] Ancuti M.C., Tutelea L., Andreescu G.D., *ET AL.*: 'Practical wide-speed-range sensorless control system for permanent magnet reluctance synchronous motor drives via active flux model', *Electr. Power Compon. Syst.*, 2014, **42**, pp. 91–102

[28] Zhao Y., Zhang Z., Qiao W., *ET AL.*: 'An extended flux model-based rotor position estimator for sensorless control of salient-pole permanent-magnet synchronous machines', *IEEE Trans. Power Electron.*, 2015, **30**, pp. 4412–4422

[29] Kalluf F.J.H., Isfanuti A.S., Tutelea L.N., *ET AL.*: '1-kW 2000–4500 r/min ferrite PMSM drive: comprehensive characterization and two sensorless control options', *IEEE Trans. Ind. Appl.*, 2016, **52**, pp. 3980–3989

[30] Haitham A.R., Atif I., Jaroslaw G.: 'High performance control of AC drives with Matlab/Simulink models' (Wiley, 2012)

[31] Ren J.J., Liu Y.C., Wang N., *ET AL.*: 'Sensorless control of ship propulsion interior permanent magnet synchronous motor based on a new sliding mode observer', *ISA Trans.*, 2015, **54**, pp. 15–26

[32] Spurgeon S.K.: 'Sliding mode observers: a survey', *Int. J. Syst. Sci.*, 2008, **39**, pp. 751–764

[33] Krishna M., Daya F.J.L.: 'Adaptive speed observer with disturbance torque compensation for sensorless induction motor drives using RT-Lab', *Turk. J. Elec. Eng. Comp. Sci.*, 2016, **24**, pp. 3792–3806